Progress In Electromagnetics Research Letters, Vol. 113, 25–34, 2023

Compact Broadband Dual-Polarized Antenna with Parasitic Patches

Sensen Han, Feng Shang*, and Xinwei Wang

Abstract—In this paper, a broadband compact dual-polarized antenna for base stations is proposed. This antenna consists of a pair of crossed dipoles, four triangular parasitic patches, and a box reflector. The crossed dipoles are fed by two 50 Ω coaxial cables. The increase of four parasitic patches allows the resonant point to be generated at high frequencies to further widen the impedance bandwidth; the size of the parasitic patches is reduced to realize the reduction of the antenna radiator size; and the impedance matching is improved by cutting circular slots in the dipole arms. The measured results show that the proposed antenna is able to achieve a wide impedance bandwidth of 79% (1.67 to 3.87 GHz) with VSWR less than 1.6. A stable gain of 8–8.7 dBi and a half-power beamwidth (HPBW) of 60–78° are obtained at 2.2–3.65 GHz. In addition, the antenna radiator is very compact in size, only about $0.41\lambda_L \times 0.41\lambda_L \times 0.17\lambda_L$, where λ_L is the longest operating wavelength.

1. INTRODUCTION

With the rapid development of wireless communication systems, more and more communication standards (e.g., 2G, 3G, 4G, 5G) have coexisted for a long time, and the design of wideband, dual-polarized antennas is strictly required to save installation space and operation and maintenance costs of base stations. In addition, in many practical applications, space constraints increase the importance of reducing antenna size. However, wide bandwidth and compactness are often contradictory, and most broadband antennas are relatively large in size, at least half wavelength. However, compact antennas usually have a narrow bandwidth [1].

Among the existing antenna types, the crossed dipole antenna has the advantages of wide bandwidth, dual polarization, and simple structure, which is a good choice to meet all the above requirements at the same time. To further improve the bandwidth of the antenna, in [2], a loop dipole antenna with a Y-shaped feed line is proposed to achieve a 27.8% dual-polarization bandwidth. A differentially fed dual-polarized patch antenna with four pairs of parasitic elements introduced to increase the bandwidth is proposed in [3], which achieves 45% of the 15 dB impedance bandwidth ($|S_{dd11}| < -15$ dB). Antenna radiator size is $0.44\lambda_L \times 0.44\lambda_L \times 0.23\lambda_L$. In [4] and [5], researchers use an additional feed balun to increase the impedance bandwidth to 67% and 75%, respectively. However, the additional feed balun-unbalun converter is located between the antennas and has a more complex structure. Although the dual-polarized slit antennas proposed in [6] and [7] have a wide impedance bandwidth (45.8% and 38.7%, respectively), they both have a large aperture size ($1.1\lambda_L \times 1.1\lambda_L$ and $0.51\lambda_L \times 0.51\lambda_L$, respectively) due to the natural characteristics of slit antennas. In [8], a broadband multi-microstrip dipole antenna is proposed, achieving an impedance bandwidth of 48.3% ($|S_{dd11}| < -10$ dB) with an antenna radiator size of $0.59\lambda_L \times 0.59\lambda_L \times 0.14\lambda_L$.

Recently, in [9], a design of broadband dual-polarized antenna using short dipole, integrated balun, and cross-feed is proposed, which has an impedance bandwidth of 74.5% (1.69–3.7 GHz) at

Received 17 July 2023, Accepted 18 October 2023, Scheduled 27 October 2023

* Corresponding author: Feng Shang (shangfeng@xupt.edu.cn).

The authors are with the College of Electronic Engineering, Xi'an University of Posts and Telecommunications, Xi'an 710121, Shaanxi, China.

VSWR < 1.5 for both ports, with good radiation characteristics in 2G/3G/4G base station bands (1.7–2.7 GHz). In [10], a wide-beam dual-polarized antenna is presented, using parasitic elements to increase the impedance bandwidth, and the proposed antenna has 61% impedance bandwidth. The voltage standing wave ratio (VSWR) is < 2.0 and also has wide beam characteristics. A dipole antenna based on a fragmented structure is proposed in [11]. The optimized crossed dipole antenna can obtain a wide operating bandwidth of 76.3%, and the whole antenna size (including the reflector plate) is about $0.75\lambda_L \times 0.75\lambda_L \times 0.16\lambda_L$.

In this letter, we propose a compact crossed dipole antenna with a parasitic patch. By improving the basic crossed dipole in [12], a new structure is obtained, where the introduction of the parasitic patch introduces a resonance point at high frequencies, and circular slots are cut in the dipole arms to improve the impedance matching deterioration after the parasitic patch is reduced. The conventional planar reflector is replaced by a box-shaped reflector to stabilize the gain at high frequency. The proposed antenna is able to achieve a wide impedance bandwidth of 79% (1.67–3.87 GHz) with voltage standing wave ratio (VSWR) less than 1.6. A stable gain of 8–8.7 dBi and a half-power beamwidth of 60–78° at 2.20–3.65 GHz are obtained.

2. ANTENNA DESIGN

2.1. Antenna Configuration

The antenna configuration is shown in Figure 1. The antenna consists of three parts, crossed dipoles, four parasitic patches, and a boxed reflector. Both the parasitic patches and the dipole are printed on an F4BM substrate with a relative permittivity of $\varepsilon_r = 3.5$, loss tangent of 0.003, and thickness of 0.8 mm. One arm of the dipole and the four parasitic patches are printed on the front side of the F4BM substrate, while the other arm is printed on the back side of the F4BM. Each dipole is excited by a feeder coaxial cable whose outer conductor is connected to one of the dipole arms printed on the back side of the F4BM substrate, and the inner conductor is connected to the other arm via a microstrip line. To obtain a stable radiation pattern, a box reflector is used instead of a conventional reflector at a distance of 30 MM (about $0.17\lambda_L$, where λ_L is the longest operating wavelength). Detailed parameter dimensions are listed in Table 1.

The designed antenna employs a dipole antenna with semicircular arms instead of a conventional dipole because semicircular dipoles have a wider impedance bandwidth, and the length of a single dipole arm is about $0.5\lambda_0$ (where λ_0 is the free-space wavelength at the center frequency of 2.76 GHz). The

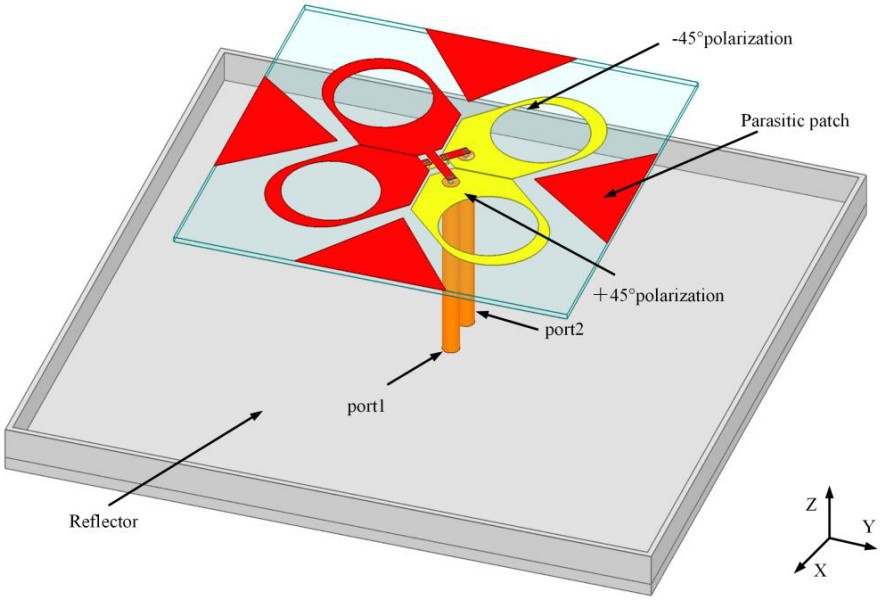

(a)

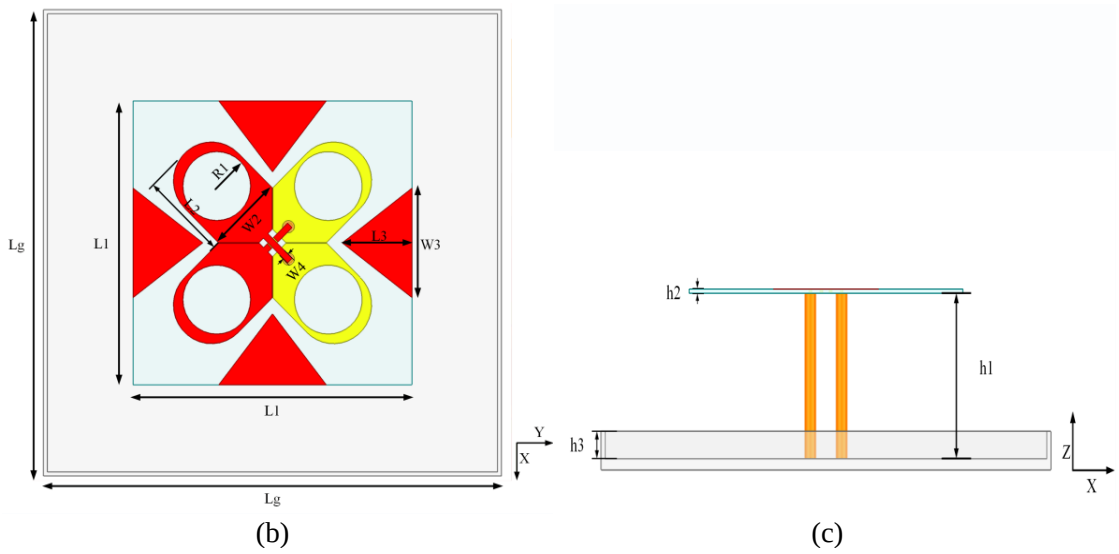

Figure 1. Geometry of the proposed antenna. (a) Three-dimensional view. (b) Top view. (c) Side view.

Table 1.

Parameters	Lg	$L1$	$W2$	$L2$	$W3$
Value (mm)	115	74	19.8	21.9	30
Parameters	$R1$	$L3$	$W4$	$H1$	$H2$
Value	8.9	19	1.6	30	0.8
Parameters	$H3$				
Value	5				

length of the added triangular parasitic patch $l3$ around the periphery is 19 mm (which is the free-space wavelength at 3.9 GHz, approximately). $W4$ corresponds to a microstrip line width of 50 Ω. The dimensions of the floor were optimized by simulation, and the optimal size of 115 mm was determined to ensure the stability of the radiation pattern.

2.2. Evolution of Antenna

To better illustrate the design concept of this dipole antenna, the evolution of the antenna is shown in Figure 2. In the first step, antenna A is the initial crossed dipole antenna with a semicircular arm, two 50 Ω coaxial cables, and a metal reflector, as shown in Figure 2(a). In the second step, four triangular parasitic patches are added around the crossed dipole of antenna A, called antenna B, as shown in Figure 2(b), and in the third step, a circular slot is cut in each radiating arm of antenna B, called antenna C, as shown in Figure 2(c). Finally, the conventional square reflector plate is replaced by a box-shaped reflector plate, called antenna D, as shown in Figure 2(d).

Figure 3(a) shows the VSWR results for the +45° polarization of these different antennas. The VSWR results for the −45° polarization are not shown due to the symmetric structure. For antenna A, with good impedance matching the VSWR is less than 1.5 in the range of 1.79–3.13 GHz. For antenna B, by adding four triangular parasitic patches around the dipole arm to create a resonant point at high frequency, the VSWR is less than 2 in the range of 1.52–3.84 GHz. Figure 3(b) shows the effect of parameter $L3$ on the VSWR of antenna B. It can be seen from the figure that when the size of the parasitic patch $L3$ is decreasing, the high frequency resonance point starts to move to higher frequencies, and at the same time the matching of the high frequency part starts to get worse. However,

in mobile communication systems, the antenna VSWR is generally required to be less than 1.5, and the introduction of the parasitic patch makes the antenna radiator size $0.51\lambda_L \times 0.51\lambda_L \times 0.17\lambda_L$. In order to enhance the impedance matching, while reducing the size of the parasitic patch, antenna C is introduced. In antenna C, the circular slot is cut on the basis of the original dipole arm, and the size of

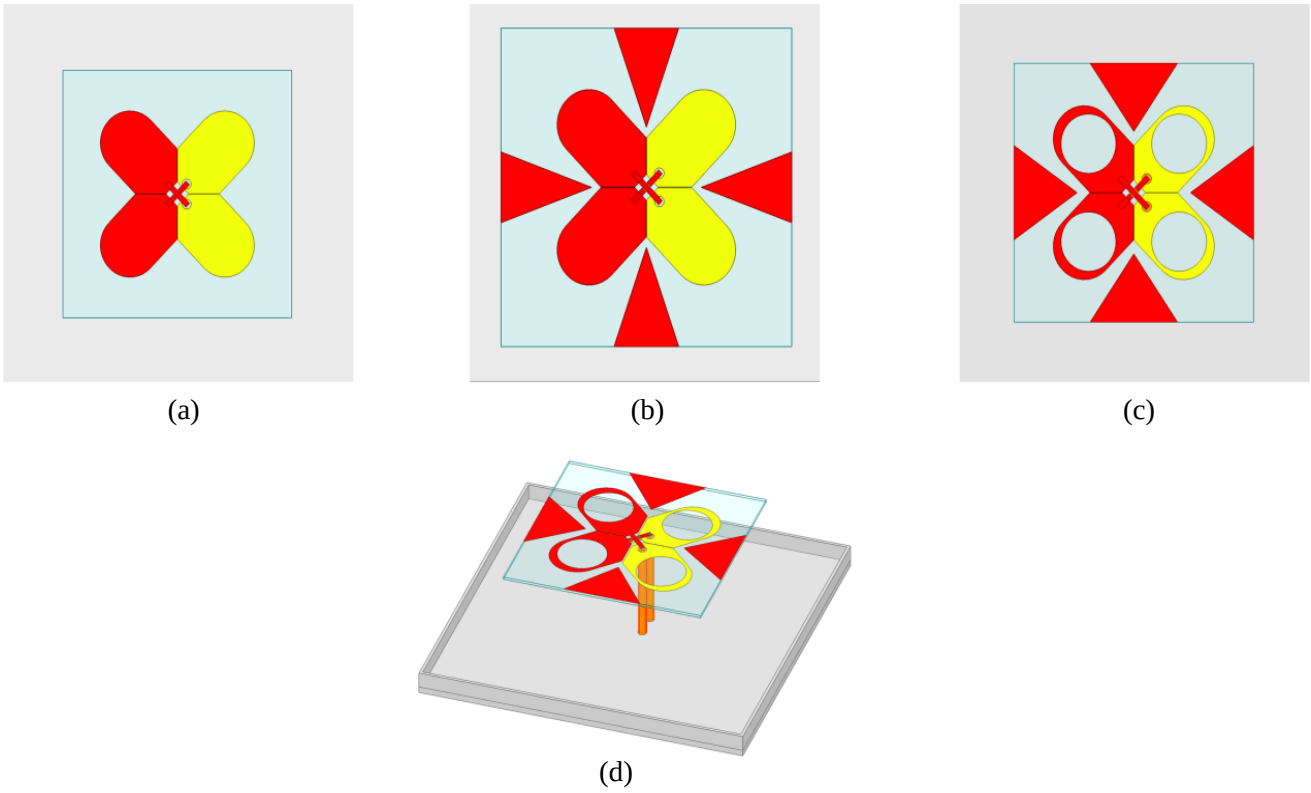

Figure 2. Five configuration processes. (a) Antenna A. (b) Antenna B. (c) Antenna C. (d) Antenna D.

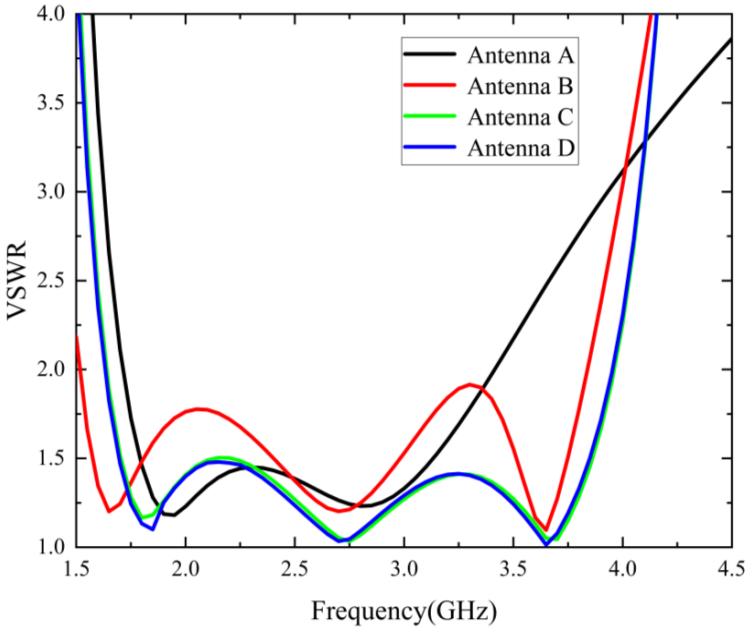

(a)

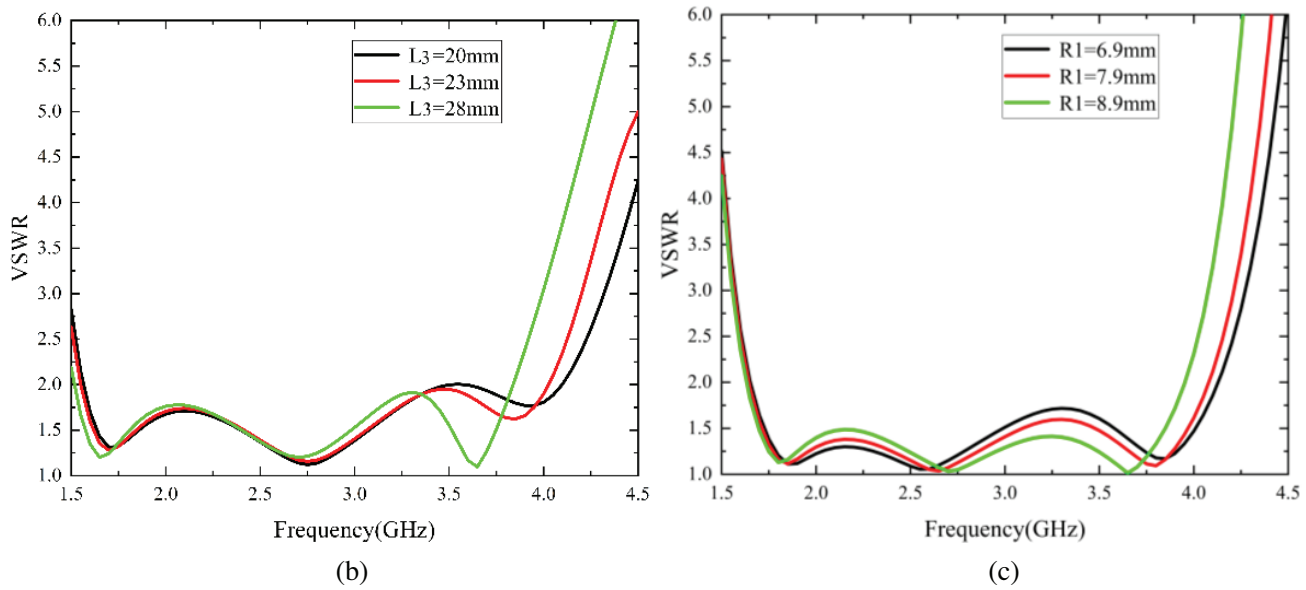

Figure 3. Four configuration processes. (a) Simulated VSWRs of antenna A, antenna B, antenna C, and antenna D. (b) Effect of parasitic patch parameter $L3$ in antenna B on VSWR. (c) Effect of circular slot parameter $R1$ in antenna C on VSWR.

the parasitic patch is reduced at the same time. The increase of the circular slot makes the VSWR less than 1.5 in the range of 1.7–3.85 GHz. Figure 3(c) shows the effect of parameter $R1$ on the VSWR of antenna C. From Figure 3(c), it can be seen that the matching at high frequency keeps getting better when the radius of the circular slot $R1$ keeps increasing, and the matching reaches the optimum when $R1 = 8.9$ mm. At the same time, the size of radiator is changed from 90 mm to 74 mm, which makes the structure more compact. In antenna D, the traditional flat reflector is replaced by a box-shaped reflector, and the high frequency gain is improved, while the beamwidth is stabilized.

In order to obtain a stable radiation pattern, the effect of different antenna parameters on the antenna gain and beamwidth is investigated. On the basis of antenna C, the original square reflector plate was changed into a boxed reflector plate. Antenna D was proposed with a height of $H2 = 5$ mm around the metal, and as can be seen from Figure 4(a), the gain of the antenna at high frequencies was improved after adding the metal surround. The variation of beamwidth before and after the change of reflector plate is shown in Figure 4(b). Antenna D has a stable gain of 8–8.7 dBi from 1.7 GHz to 3.7 GHz and 5.9 dBi at 3.85 GHz. The half-power beamwidth is also stable in the 2.2 GHz–3.65 GHz band within 60–78°.

2.3. Antenna Mechanism

To better understand the working principle of the proposed antenna, Figure 5 shows the current distribution at 1.8, 2.7, 3.65, and 3.85 GHz when port 1 of the antenna is excited. Due to the symmetrical structure, the current distribution when port 2 is excited is not shown here. At the resonant frequency of 1.8 GHz, the current is mainly concentrated on the +45° polarized dipole, with relatively weak currents in the surrounding triangular parasitic patches. At 2.7 GHz, the currents on the two pairs of dipole arms are significantly enhanced, when the radiation capability is stronger. When the frequency is 3.65 GHz, the surrounding triangular parasitic patch produces a stronger induced current in anti-phase with the +45° polarizatized dipole, and the resonant modes at the high frequency, which are mainly generated by the coupling between the dipole and the triangular parasitic patch, cancel each other's radiated field due to the anti-phase of the produced currents, which means that the radiative characteristics at the high frequency will be reduced.

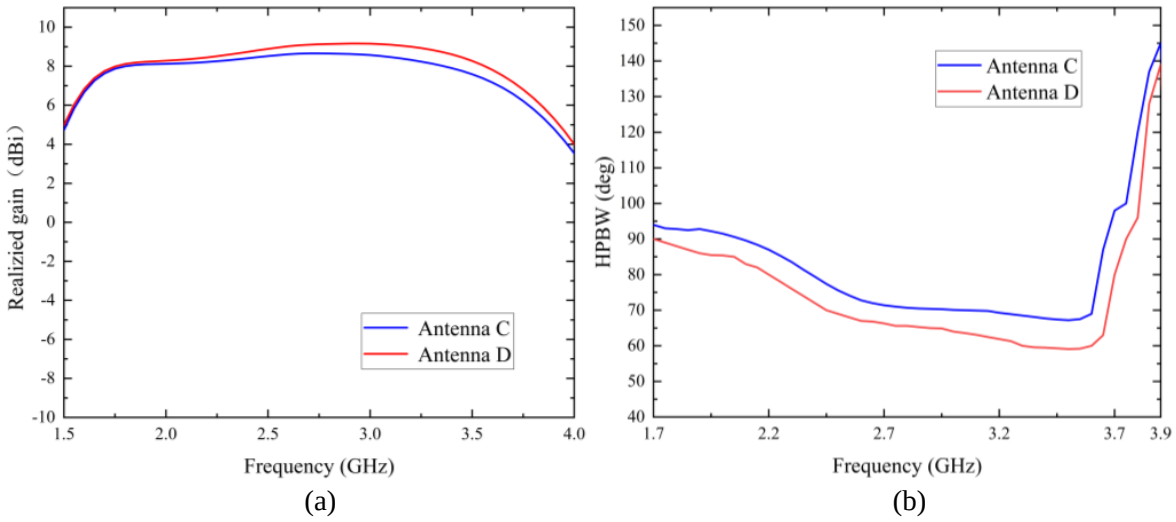

Figure 4. (a) Simulated realized gains of the antennas C and D. (b) Simulated HPBWs of antennas C and D.

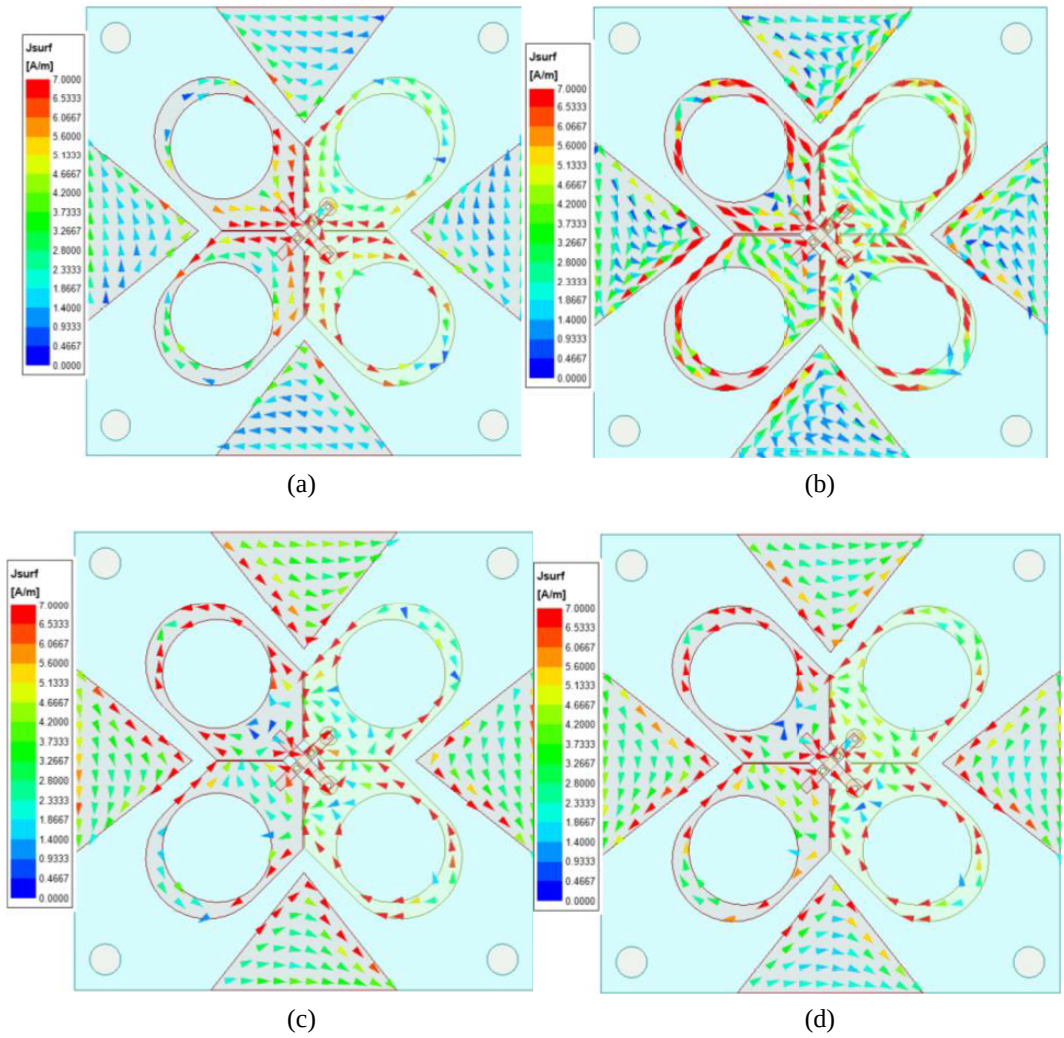

Figure 5. Current distributions of the antenna. (a) 1.8 GHz. (b) 2.7 GHz. (c) 3.65 GHz. (d) 3.85 GHz.

3. SIMULATION AND EXPERIMENTAL RESULTS

In order to validate the proposed design, a prototype of the proposed antenna was fabricated and measured. Figure 6(a) shows the actual model and test scenario of the proposed antenna. E5063A vector network analyzer was used to test the voltage standing wave coefficient, and Figure 6(b) shows the antenna gain and far-field radiation pattern measured in a microwave anechoic chamber.

A photograph of the fabricated antenna is shown in Figure 7. The simulated and measured VSWRs are provided in Figure 8. The impedance bandwidth for port 1 is 79% (from 1.67 GHz to 3.87 GHz) when VSWR < 1.6. The VSWR of port 2 is slightly higher than that of port 1 over the entire bandwidth. This is due to the overbore configuration used to avoid intersection. The measured results are slightly better than the simulated ones due to manufacturing tolerances. Figure 9 shows the measured and simulated isolations in the operating band of the proposed antenna. The isolation of both ports exceeds 20 dB over the entire bandwidth range.

Figure 10 shows the measured gain and HPBW in the horizontal plane. The measured gain is about 1 dB lower than the simulated one over the entire band range, mainly due to feeder cable losses and measurement errors. From 2.2 GHz to 3.65 GHz, the measured HPBW ranged from 60° to 78°, with the gain ranged from 8 dBi to 8.7 dBi. In measurements at 3.7 GHz, the HPBW increases to 90°, and the gain decreases to 7.1 dBi. Figure 11 gives the H-plane and the simulated and measured normalized radiation patterns at different frequencies. Due to the symmetry of the structure, only +45° polarization

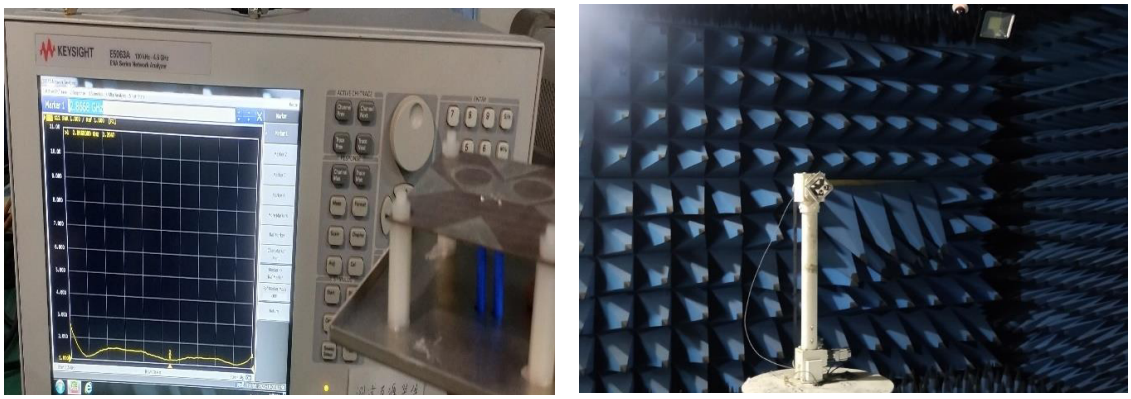

(a) (b)

Figure 6. Antenna to be measured in Vector Network Analyzer and microwave chamber.

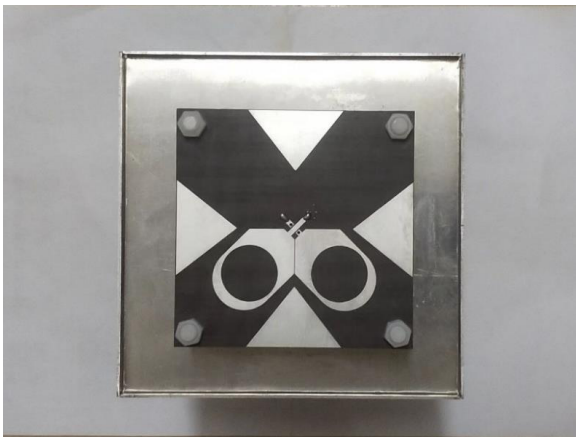

Figure 7. Prototype of the proposed antenna.

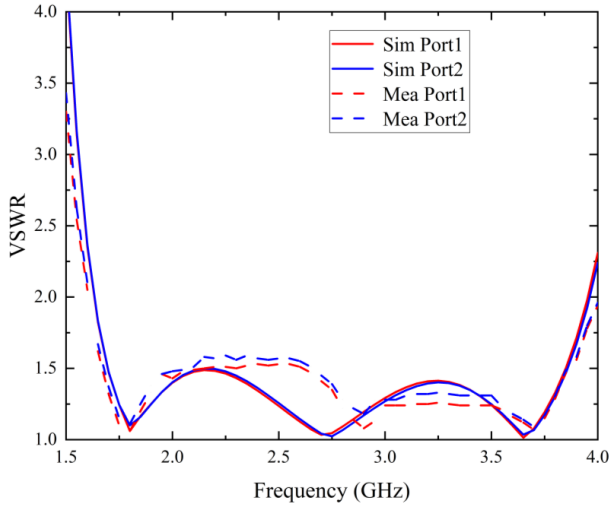

Figure 8. Simulated and measured VSWRs of the proposed antenna.

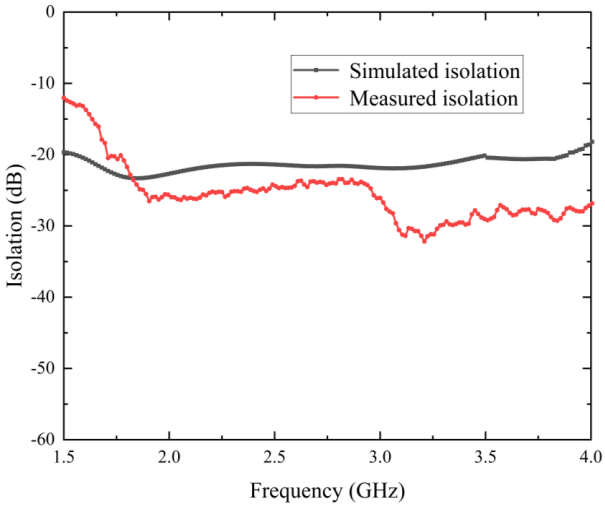

Figure 9. Simulated and measured isolations of the proposed antenna.

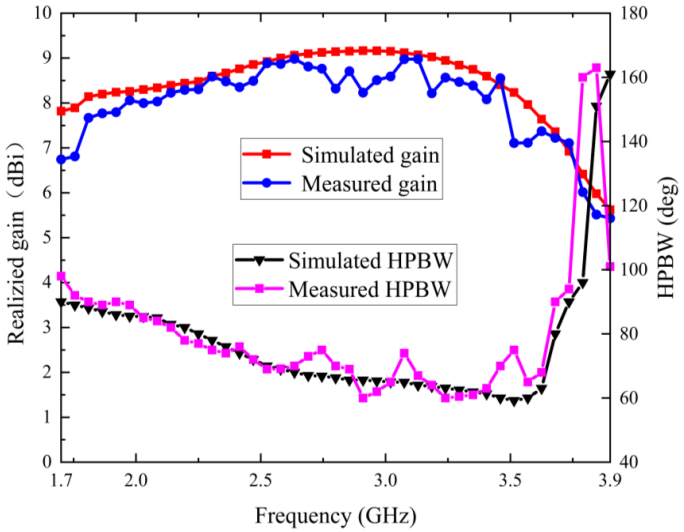

Figure 10. Simulated and measured gain and HPBWs of the proposed antenna.

Table 2.

Ref.	Bandwidth	Gain (dBi)	Size of radiator	Size of antenna (with reflector)
[3]	45% ($S_{11} < -15$ dB)	9	$0.44\lambda_L \times 0.44\lambda_L \times 0.23\lambda_L$	$0.91\lambda_L \times 0.91\lambda_L \times 0.23\lambda_L$
[4]	67% ($S_{11} < -15$ dB)	7.9 ± 1	$0.43\lambda_L \times 0.43\lambda_L \times 0.28\lambda_L$	$0.68\lambda_L \times 0.68\lambda_L \times 0.28\lambda_L$
[8]	48% ($S_{11} < -10$ dB)	8.9 ± 0.7	$0.78\lambda_L \times 0.78\lambda_L \times 0.\lambda_L$	$0.78\lambda_L \times 0.78\lambda_L \times 0.\lambda_L$
[11]	76.3% ($S_{11} < -15$ dB)	9 ± 0.65	$0.31\lambda_L \times 0.31\lambda_L \times 0.31\lambda_L$	$0.75\lambda_L \times 0.75\lambda_L \times 0.16\lambda_L$
Prop.	79% (VSWR < 1.6)	8–8.7	$0.41\lambda_L \times 0.41\lambda_L \times 0.17\lambda_L$	$0.65\lambda_L \times 0.65\lambda_L \times 0.17\lambda_L$

λ_L is the free-space wavelength at the lowest frequency of the operating bands.

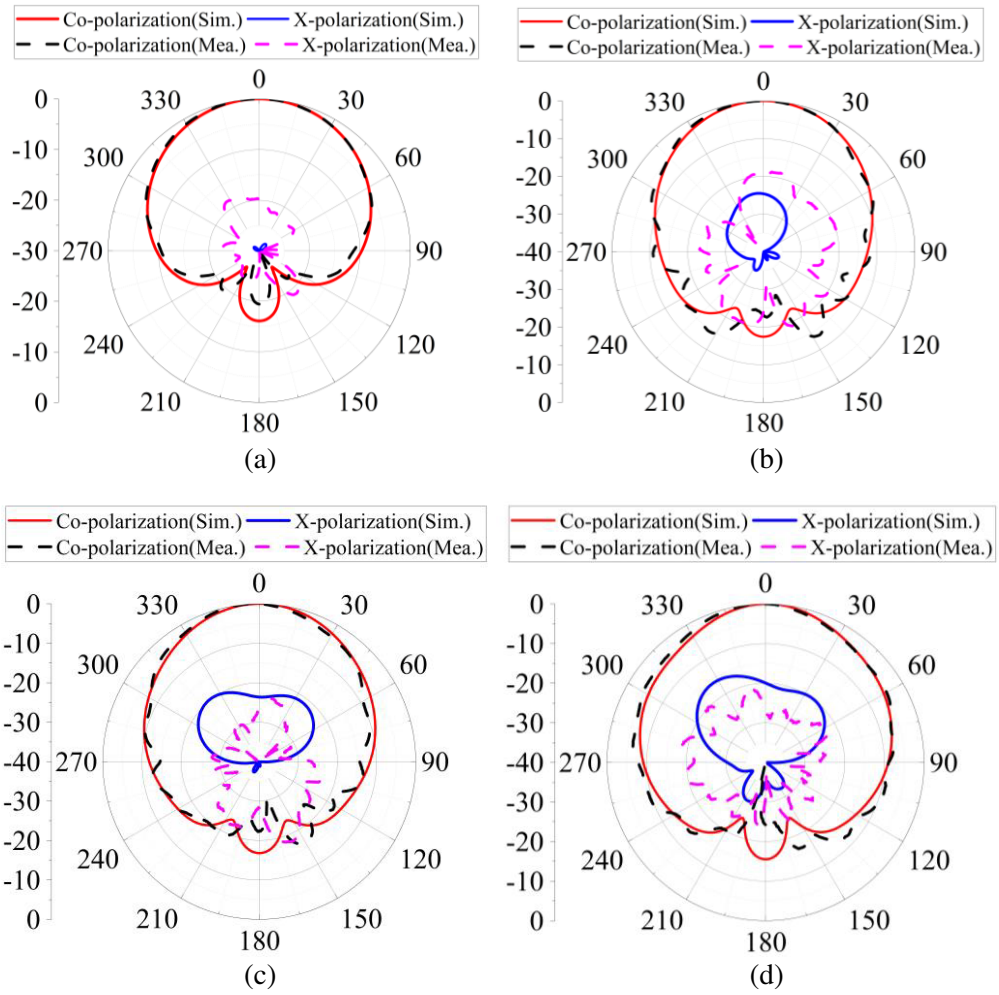

Figure 11. Simulated and measured radiation patterns for +45° polarization in the *H*-plane. (a) 1.8 GHz. (b) 2.6 GHz. (c) 3 GHz. (d) 3.4 GHz.

is provided. It is observed that the measured results are in good agreement with the simulated ones.

Table 2 lists the comparison of this work with other broadband dual-polarized antennas. Compared to the antennas in [3] and [8], our antenna has the advantage of a much wider operating bandwidth. Compared to the broadband dual polarized antenna in [4], our antenna has smaller radiator size and wider bandwidth. Compared to the antenna in [11], our work has a much wider bandwidth and a smaller overall antenna size (including the reflector). These features make it attractive for base station applications.

4. CONCLUSION

In this paper, a compact broadband dual-polarized antenna is proposed, introducing parasitic patches to broaden the impedance bandwidth, adding circular slots to improve the match deterioration after reducing the size of parasitic patches, reducing the radiator size and making the structure more compact. Simulation and measurement results show that the proposed antenna has a VSWR < 1.6 in the 1.67–3.87 GHz range and achieves 79% broadband characteristics. It can fully cover 5G NR-n41/78 frequency band. With these required characteristics, the proposed antenna will find potential in practical base station applications.

REFERENCES

1. Li, J., S.-J. Hao, Y.-G. Cui, and X. Chen, "A miniaturized wideband dual-polarized planar antenna based on multiresonance," *IEEE Antennas and Wireless Propagation Letters*, Vol. 21, No. 2, 242–246, Feb. 2022.
2. Wen, D.-L., D.-Z. Zheng, and Q.-X. Chu, "A dual-polarized planar antenna using four folded dipoles and its array for base stations," *IEEE Transactions on Antennas and Propagation*, Vol. 64, No. 12, 5536–5542, Dec. 2016.
3. Cui, Y., X. Gao, and R. Li, "A broadband differentially fed dual-polarized planar antenna," *IEEE Transactions on Antennas and Propagation*, Vol. 65, No. 6, 3231–3234, Jun. 2017.
4. Sun, H. H., C. Ding, H. Zhu, and Y. J. Guo, "Dual-polarized multi-resonance antennas with broad bandwidths and compact sizes for base station applications," *IEEE Open J. Antennas Propag.*, Vol. 1, 11–19, 2019.
5. Fu, S., Z. Cao, X. Quan, and C. Xu, "A broadband dual-polarized notched-band antenna for 2/3/4/5G base station," *IEEE Antennas and Wireless Propagation Letters*, Vol. 19, No. 1, 69–73, Jan. 2020.
6. Jiang, X., Z. Zhang, Y. Li, and Z. Feng, "A wideband dual-polarized slot antenna," *IEEE Antennas and Wireless Propagation Letters*, Vol. 12, 1010–1013, 2013.
7. Lian, R., Z. Wang, Y. Yin, J. Wu, and X. Song, "Design of a low-profile dual-polarized stepped slot antenna array for base station," *IEEE Antennas and Wireless Propagation Letters*, Vol. 15, 362–365, 2016.
8. Zhou, Z., Z. Wei, Z. Tang, and Y. Yin, "Design and analysis of a wideband multiple-microstrip dipole antenna with high isolation," *IEEE Antennas and Wireless Propagation Letters*, Vol. 18, No. 4, 722–726, Apr. 2019.
9. Wen, L.-H., et al., "A wideband dual-polarized antenna using shorted dipoles," *IEEE Access*, Vol. 6, 39725–39733, 2018.
10. Feng, Y., F.-S. Zhang, G.-J. Xie, Y. Guan, and J. Tian, "A broadband and wide-beamwidth dual-polarized orthogonal dipole antenna for 4G/5G communication," *IEEE Antennas and Wireless Propagation Letters*, Vol. 20, No. 7, 1165–1169, Jul. 2021.
11. Wang, D., G. Wang, D. Lu, N. Yang, and Q. Zhang, "Design of wideband base station antenna by involving Fragment-type structures on dipole arms," *IEEE Transactions on Antennas and Propagation*, Vol. 70, No. 7, 5953–5958, Jul. 2022.
12. Ye, L. H., Y. J. Li and D.-L. Wu, "Dual-wideband dual-polarized dipole antenna with T-shaped slots and stable radiation pattern," *IEEE Antennas and Wireless Propagation Letters*, Vol. 21, No. 3, 610–614, Mar. 2022.